

Resonant excitation series at the Kr 3*p* and Xe 4*p* thresholds

I. T. Steinberger

Racah Institute of Physics, The Hebrew University, Jerusalem 91904, Israel

C. M. Teodorescu,* D. Gravel, and R. Flesch

Fachbereich Physik, Universität Osnabrück, Barbarastrasse 7, D-49069 Osnabrück, Germany

B. Wassermann

Fachbereich Chemie, Freie Universität Berlin, Takusstrasse 3, D-14195 Berlin, Germany

G. Reichardt

BESSY GmbH, Lentzeallee 100, D-14195 Berlin, Germany

C. W. Hutchings

Behlen Laboratory of Physics, University of Nebraska, Lincoln, Nebraska 68588-0111

A. P. Hitchcock

Department of Chemistry, McMaster University, Hamilton, Ontario, Canada L8S 4M1

E. Rühl

Fachbereich Physik, Universität Osnabrück, Barbarastrasse 7, D-49069 Osnabrück, Germany

(Received 16 December 1998)

A systematic comparison is presented between the gas-phase and solid-phase features of the resonant core excitation series in 3*p* excited krypton and 4*p* excited xenon. For the gases total ion yield spectra were recorded. For the solids, photoemission yield (total electron yield) spectra were complemented with photoconductivity excitation spectra, recording electron transport in the conduction band. The gas-phase spectra were compared with predictions of recent theoretical work [M. Ohno, *Phys. Rev. A* **51**, 1042 (1995)] and approximated by means of the simple Rydberg formula with constant quantum defect. The core excitation series observed in the solids are analogous to the Mott-Wannier valence exciton series, as transitions from the respective core levels into the lowest conduction band are dipole allowed. Similar to the case of valence excitons, the series limit of these core excitons was found to correspond to a rise in the photoconduction signal, marking the onset of direct transitions into the conduction band. However, the core exciton energies are close to the gas-phase Rydberg state energies, in contrast with the valence excitons that have binding energies considerably smaller than the respective valence Rydberg states in the gas. The energies of the core excitons observed cannot be described by means of the effective reduced exciton mass and the dielectric constant: the simple Mott-Wannier effective-mass model is inadequate for these excitons. [S0163-1829(99)09529-6]

I. INTRODUCTION

Haensel *et al.* reported results of systematic and extensive studies of soft x-ray absorption spectra of rare gases in both the gas and solid phases.¹⁻⁴ Their investigations revealed that though just below each absorption edge the spectra in the two phases are basically similar, the lines in the solids ("core excitons") are broadened and systematically blue-shifted compared with the atomic Rydberg states observed in the gases. These results are consistent with more recent investigations of free rare-gas clusters in the same energy range⁵⁻¹⁰ that bridge between the gas and the solid phases and encompass the two phases as limiting cases. These studies distinguish very clearly between surface and bulk features; e.g., for the Kr 3*d* edge region¹⁰ shifts of core excitons with cluster size give specific information about the distance of the excited atom from the surface and about surface sites.

Previous works¹⁻¹⁰ dealt predominantly with spectral re-

gions where strong variations of the absorption cross section occur. In contrast, this work concerns the Kr 3*p* and Xe 4*p* absorption edge regions, where variations of the cross section become manifest as weak structures sitting on top of intense absorption continua. The main motivation for the study has been the fact that transitions from subshells with *p* symmetry in the solid rare gases have interesting analogs in the valence regime: we looked for core excitons analogous to Wannier-Mott excitons. The latter are states where a hole from a *p*-like valence band is coupled, by screened Coulomb interaction, to an electron of the *s*-like lowest conduction band. Similarly, a Kr 3*p* or Xe 4*p* core hole may form a core exciton by coupling to an electron of the 5*s* or 6*s* conduction band, respectively. In contrast, excitations from *d* or *s* cores have no simple valence Mott-Wannier exciton analogs, since transitions from such shells to the bottom of the *s*-like conduction band are dipole forbidden. Among core excitons associated with transitions from *p* subshells Haensel *et al.*

studied transitions from Ar $2p$ (Refs. 3 and 4) and Xe $4p$.² Near the Ar $2p$ thresholds they identified two of the observed lines, corresponding to the $2p_{3/2} \rightarrow 4s$ and $2p_{1/2} \rightarrow 4s$ atomic transitions, as Frenkel excitons.^{3,4} Accurate determination of the peak positions and the assignment of higher lines is rather difficult for solid Ar, since the lines are lifetime broadened^{11,12} and the spin-orbit splitting is appreciably smaller than the binding energies of the lowest Rydberg states -2.12 eV (Ref. 13) vs 4 eV.^{3,13} As a result, some members belonging to different series overlap or even blend. In solid xenon, poorly resolved small peaks near the $4p$ edges were reported.²

In this work particular emphasis was laid on comparing results for each substance, (i) in the solid and gas phase, and (ii) between core and corresponding valence excitations. This double aim could be achieved thanks to improved resolution and statistics, leading to the observation of better defined lines for Kr gas and of more lines, with higher resolution, for Xe gas and solid; for Kr solid at the $3p$ threshold, the present work contains, to our knowledge, the first published results. The results for the gases were compared to basic theory.¹⁴ In order to test whether simple semiempirical models are applicable for core excitation series, we also checked to what extent are simple series laws useful approximations for the peak positions.

Total ion yield (TIY) spectroscopy served for the study of the gases. For the solids, photoemission yield (or total electron yield) and photoconductivity excitation spectra were simultaneously recorded. The latter method is directly affected by the band structure of the solid, as it records electron propagating in the conduction band. In the valence regime, for solid and liquid rare gases, the band-gap energy¹⁵ as well as the adiabatic ionization energies of various impurities¹⁶ were directly determined by this method, while they could not be directly observed as edges in the absorption and reflection spectra because of the very high exciton oscillator strengths.¹⁷ The photoemission yield and photoconduction excitation spectra were expected to differ in the spectral region where photoelectrons are directly liberated, but it has also been clear from the outset that electrons originating in Auger or Coster-Kronig core decay processes and their secondaries, might obscure to some extent the differences.

II. EXPERIMENT

Monochromatic synchrotron radiation at BESSY-I was employed for all the measurements: for the Kr $3p$ edge region from the monochromator HE-TGM-2,¹⁸ with an energy resolution of ~ 400 , and for the Xe $4p$ edge region from the monochromator U2-FSGM (Ref. 19) with an energy resolution of 5000 . For the gas phase, total ion yields were measured by continuous extraction of the cations from the ionization region of a time-of-flight mass spectrometer.⁵ The typical pressure in the ionization region was about 10^{-5} mbar.

The solid samples were prepared on a sapphire cold finger within a closed circuit He refrigerator cryostat. The base pressure was in the range of a few times 10^{-8} Pa. Two par-

allel gold stripes, prepared by vacuum deposition, with a distance of 2 mm in between, served as contacts and enabled photoconduction measurements on the samples. A procedure of pumping, baking, and cooling down to below 20 K preceded the sample deposition. A stainless-steel platelet, mounted parallel to the sapphire base at a distance of 10 mm, served as collector electrode for the photoemission yield (or total electron yield) measurements. Monochromatic synchrotron radiation reached the sample through a 3 -mm-wide slit in the collector electrode. The photocurrents measured were in the 10^{-13} – 10^{-9} A range. The spectral intensity distribution of the incident radiation was monitored simultaneously with the sample spectra by means of a photodiode with a gold-coated grid serving as a photocathode. The spectra were normalized to equal numbers of incident photons by means of this intensity distribution.

The wavelength scale was calibrated by means of comparison with high-accuracy published data in the range of study. For the spectrum of Kr gas, the 244.39 -eV line ($2p_{1/2} \rightarrow 4s$) in Ar gas¹³ and the spectrum of SF₆ gas between 172 and 185 eV (Ref. 20) were used for reference with an uncertainty of about ± 0.1 eV. For the wavelength calibration of solid Kr, we recorded the spectrum of solid SF₆ in the above range and the line assigned to $2p_{1/2} \rightarrow 4s$ in solid argon. In the course of a study of Ar clusters of variable sizes⁹ the photon energy of this line was determined to be 245.16 eV; an early value by Haensel *et al.* was 245.2 eV.⁴ It is known from measurements on SF₆ in the gas phase,²⁰ variable size clusters²¹ and the solid phase²² that in the spectral range concerned the line positions do not depend on the phase. The calibration uncertainty for solid Kr is estimated as about ± 0.2 eV. For the spectra of both gas and solid Xe the SF₆ gas spectrum in the 172 – 185 -eV region²⁰ was used for reference. The calibration errors for the Xe gas and solid spectra were also about ± 0.2 eV.

Photoemission yield spectra of the sapphire substrate in the range 150 – 600 eV showed structure only at the K -edge region of oxygen (543.1 eV) indicating that no significant surface contamination affected the measurements. The sample gas was introduced into the chamber by means of a needle valve, and the dose was controlled by pressure and time measurements. Analysis of the photoconduction and photoemission results on samples prepared with very small doses indicated that 1 L corresponded *very roughly* to about one monolayer for both gases. The samples were annealed at about 30 K before starting the measurements. All spectra were taken on freshly deposited samples, since they tended to undergo slow degradation with time due to surface contamination, radiation damage, etc.

III. RESULTS AND DISCUSSION

A. Spectra

Figure 1 shows the spectrum in the gas and solid phases at the $3p$ edge region of krypton. The solid sample was made by the deposition of 70 L Kr. The spectra as obtained (after normalization to equal numbers of incident photons) appear in the insets. They are superimposed on top of a broad con-

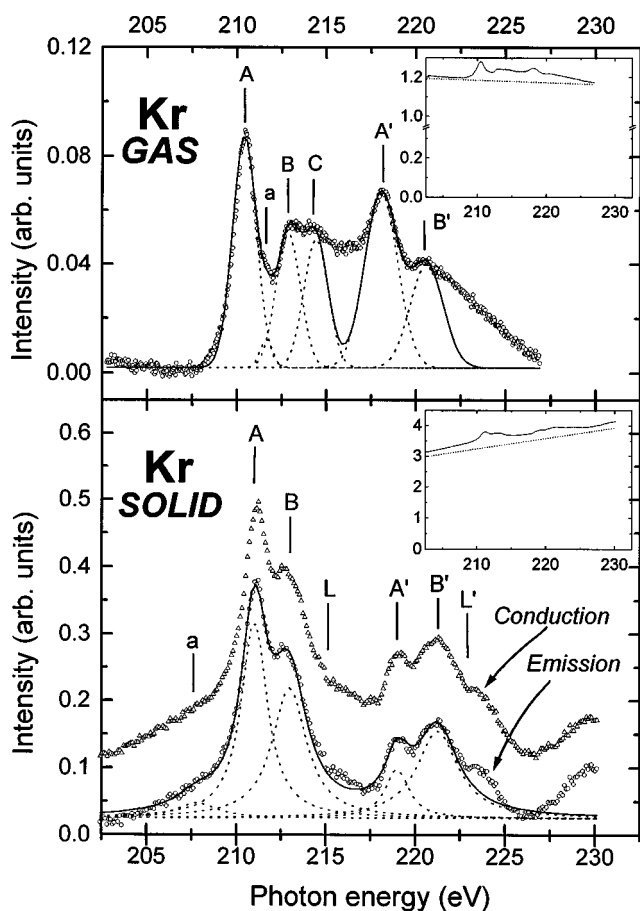


FIG. 1. Upper graph, total ion yield (TIY) spectrum of Kr gas. Lower graph, photoemission yield [or total electron yield (TEY)] and photoconduction excitation spectra of solid Kr, all with straight baselines (marked on the insets) subtracted. Range: 200–235 eV. Insets: TIY and photoemission yield spectra, without subtraction of the $3d$ continuum contribution.

tinuum, namely, that of excitation from the Kr $3d$ subshell, with a smaller contribution from $4p$. The main graphs were constructed so as to represent essentially only the $3p$ spectrum: as a rough approximation, an appropriate straight baseline (marked) was subtracted. A detailed discussion of the graphs will follow below: at this point we are drawing attention to the fact that in the solid the photoemission yield and photoconduction excitation spectra are almost identical and that in several traits both resemble the gas spectrum.

Spectra of the $4p$ -edge region of xenon are presented in Fig. 2. On the inset of the gas-phase spectrum, two different curved baselines, marked *B11* and *B12*, are drawn. Their construction will be explained below; to draw the main graph for Xe gas *B11* was subtracted from the total intensity. The solid sample was formed by depositing a dose of 8 L. In this case too, the solid spectra are roughly similar to the gas spectrum. Unlike the case of Kr, there are also several differences between the photoemission yield and the photoconduction spectra. These will be discussed further on.

The photon energies of the peaks were determined by fitting the photoemission yield spectra with a series of lines with fixed shapes. The shapes were chosen so as to obtain the relative peak positions consistently and objectively, while keeping the fitting procedure simple, with a minimum

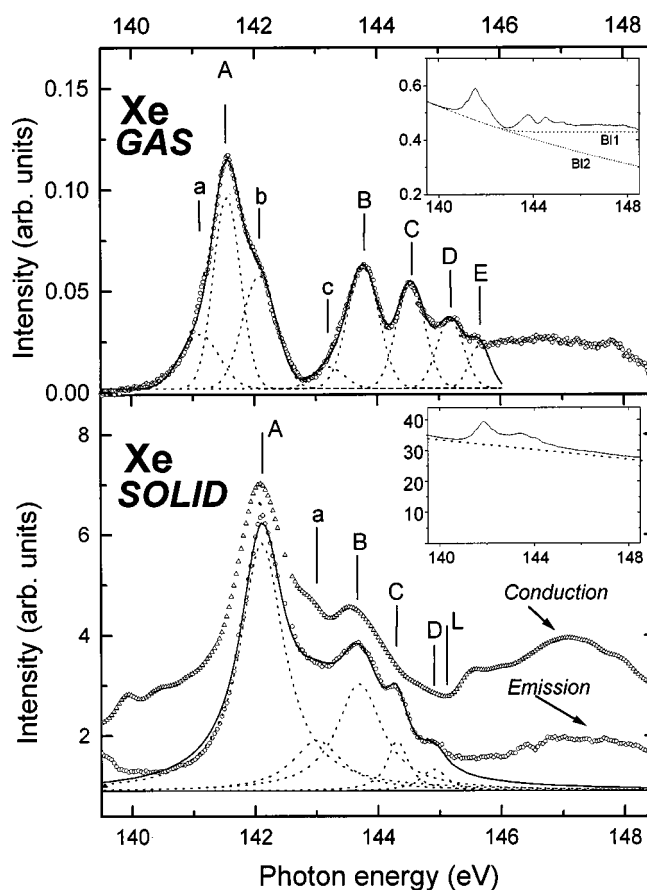


FIG. 2. Upper graph, TIY spectrum of Xe gas, with the curved baseline marked as *B11* on the inset subtracted. Lower graph, photoemission yield and photoconduction excitation spectrum of solid Xe, with straight baselines (marked in the inset) subtracted. Range: 139.5–148.5 eV. Insets: TIY and photoemission yield spectra, without subtraction of the continua contributions, see text.

number of parameters. It turned out that for the gas spectra decomposition into Gaussians was preferable, but for the solids Lorentzians gave better fits.²³ To fit the edges proper, additional parameters (four for each edge) ought to have been invoked. Their values and physical meaning could not be determined with high reliability and therefore the edges were not fitted. The relative positions of most peaks were determined in all cases to an accuracy of better than ± 0.05 eV. The error in the relative positions of the weakest peaks was somewhat larger, up to ± 0.1 eV. The accuracy of the linewidths (full width at half maximum) is stated in all cases; their error margins are usually somewhat higher than that of the peak positions. We did not attempt to determine oscillator strengths, since these depend quite strongly on the baseline subtracted and the actual (unknown) shape of the edge.

B. Kr gas

The positions of the observed peaks are presented in Table I. It can be seen that they are very near to those reported in earlier works;^{24,25} the differences are a result of calibration uncertainties in all works and of improved statistics of the present results. The peak positions were compared with those obtained by Ohno's theoretical calculations, based on the Tamm-Dancoff approximation.¹⁴ It is seen that for

TABLE I. Energies, linewidths (both in units of eV), and assignments in the TIY spectrum of Kr gas at the $3p_{3/2}$ (A , B , C , and a) and the $3p_{1/2}$ (A' and B') thresholds. Calibration uncertainty: ± 0.1 eV, relative position uncertainty: ± 0.05 eV.

Feature	Energy, expt.		Energy, calculated Eq. (1)			Assignment	FWHM	
	This work	Other works	Energy, theory	This work ^a	Other works		Expt.	Theory ^b
A	210.41	210.8 ^c 210.6 ^d	210.29 ^e	210.43		$3p^55s$	1.4 ± 0.1^f	1.88
B	212.85	213.2 ^c 213.1 ^d	212.7 ^e	213.19		$3p^56s$	1.4 ± 0.1^f	
C	214.41	213.9 ^d	213.49 ^e	214.04		$3p^57s$	1.4 ± 0.1^f	
a	211.65	211.4 ^d	212.20 ^e			$3p^54d_{3/2}$ or $3p^54d_{1/2}$	0.7 ± 0.1^f	
E_0		214.4 ^g 218.3 ^c	214.6 ^h	215.0 ± 0.4	215.0 ± 0.4^c 214.8 ± 0.3^d	$3p_{3/2}$ threshold	1.48^g	1.42
A'	218.01	218.3 ^d	218.09 ⁱ	217.94		$3p^55s'$	2.0 ± 0.1^f	2.08
B'	220.58	220.6 ^d	220.51 ⁱ	220.70		$3p^56s'$	2.0 ± 0.1^f	
E'_0		222.2 ^g	222.5 ^h	222.5 ± 0.2	222.3 ± 0.3^d	$3p_{1/2}$ threshold	1.80^g	1.89

^a $\Delta = 3.3 \pm 0.5$.

^bReference 14.

^cReference 24.

^dReference 25.

^eReference 14, taking $E_0 = 214.4$ eV (Ref. 26).

^fThis work.

^gReference 26.

^hReference 28.

ⁱReference 14, taking $E_0 = 222.2$ eV.

peaks A and B the correspondence is good, but peak C lies at an energy higher by 0.92 eV than the theoretical prediction. One reason for this discrepancy might be due to the theory becoming less accurate near the threshold.

The lines A , B , and C were assigned to $3p_{3/2} \rightarrow ns$ transitions in accord with those by Watson and Morgan²⁴ and by Ohno;¹⁴ A' and B' to $3p_{1/2} \rightarrow ns$ (Table I). On the basis of preliminary theoretical investigations Ohno¹⁴ pointed out that the $l \rightarrow l-1$ excitation is stronger than the $l \rightarrow l+1$ excitation and therefore the assignment of the lines in Ref. 25 has to be rejected. It should also be pointed out that according to our assignment the energy differences between adjacent core Rydberg states Kr $3p^5ns$ are approximately equal to the energy differences in the Rb $4p^6ns$ states. For example, the range of the $3p_{3/2}$ spectrum, i.e., the difference between the $3p_{3/2}$ binding energy²⁶ and the energy of the first line A , is 4.0 eV, while the range of the Rb $4p^6ns$ spectrum is 4.18 eV.²⁷ In contrast, according to the assignment in Ref. 25 the range of 4.2 eV in the Kr $3p_{3/2}$ spectrum would correspond to a range of 1.68-eV in the Rb $4p^6ns$ spectrum and no observed line would be assigned to $3p_{3/2} \rightarrow 5s$ transition. It should also be noted that the range of the Kr $4p_{3/2}$ spectrum is 3.97 eV,²⁷ again very near to the range of the Kr $3p_{3/2}$ spectrum, indicating that final-state interactions do not strongly affect term value differences. The assignment of the weak line a is uncertain: it might be either $3p^54d_{3/2}$ (Ref. 14) or $3p^54d_{1/2}$.

Fitting the lines A , B , and C with Gaussians yielded full widths at half height $w = 1.6 \pm 0.1$ eV. In order to determine the true width, the nominal width of the Ar $2p^54s$ line was

measured under the same conditions; it was found to be 0.69 eV. Comparing this value with 0.121 eV, determined as the true width by King *et al.*¹³ and using Lee's correction table²⁹ we established that the instrumental width was 0.62 eV. The true widths for Kr gas, namely, $w_0(A) = w_0(B) = w_0(C) = 1.4 \pm 0.1$ eV (Table I) were found by using again Lee's table. The theoretical value $w_0(A) = 1.88$ eV presented in the table was calculated by Ohno¹⁴ employing an *ab initio* Green's-function method, based on the extended random-phase approximation with exchange³⁰ for super-Coster-Kronig decay channels. The peaks of the $3p_{1/2}$ lines are broader: $w(A') = w(B') = 2.2$ eV; from this $w_0(A') = w_0(B') = 2.0 \pm 0.1$ eV, in excellent agreement with the theoretical result of 2.08 eV.¹⁴ For comparison, experimental²⁶ and theoretical¹⁴ results on the $3p_{3/2}$ and $3p_{1/2}$ hole decay widths are also shown in Table I. Other estimates of the decay width of the $3p$ holes and further references can be found in Ref. 31. As stated above, we did not attempt to fit the regions above the ionization thresholds, somewhat above C and B' , respectively. The fact that the intensity of peak C is only slightly lower than that of B might be an artifact: C is riding on the low-energy tail of the $3p_{1/2}$ edge.

Besides the experimental and theoretical results, the observed peak positions were also approximated by a simple series law, namely, as a Rydberg series with constant quantum defect Δ . In this model, for the three lines A , B , and C ,

$$E_n = E_0 - \frac{R}{(n - \Delta)^2}, \quad n = 5, 6, 7. \quad (1)$$

TABLE II. Experimental and calculated features in the photoemission yield and photoconduction excitation spectra of 3p excited solid Kr and comparisons with valence exciton energies. Calibration uncertainty, ± 0.2 eV; relative position uncertainty, ± 0.05 eV.

Feature	Energy expt.	Energy, calculated		Energy, valence excitons ^a	FWHM
		By Eq. (2) ^b	By Eq. (1) ^c		
A	210.99	210.92	210.92	10.17	1.5 \pm 0.2
B	212.96	213.03	213.03	11.23	2.1 \pm 0.2
a	207.80				2.6 \pm 0.3
L	215.1				
E_0		213.7 \pm 0.2	214.6 \pm 0.2	11.61	
A'	218.99	219.06	219.06	10.86	1.5 \pm 0.2
B'	221.24	221.17	221.17	11.92	2.7 \pm 0.2
L'	222.9				
E'_0		221.9 \pm 0.2	222.8 \pm 0.2	12.3	

^aReference 32.

^b $b = 2.8 \pm 0.2$ eV.

^c $\Delta = 3.1 \pm 0.2$.

Here R is the Rydberg constant (13.6058 eV); the series limit E_0 and the quantum defect Δ were found by fitting the equation to the experimental results. For the lines A' and B', Eq. (1) was applied with the same value of Δ , but with a different series limit E'_0 . We note that for such low Rydberg states Δ cannot be expected to be constant, especially in view of prevailing many-body effects.¹⁴ Even so, the Rydberg model proved to be a useful approximation for the spectra investigated in this work (Tables I–IV), and served as a uniform framework for comparing results in both phases.

Table I shows that the energies of peaks A, B, and C, obtained by fitting to Eq. (1), are close to the experimental ones, but there are real differences. E_0 calculated from the positions of the peaks A, B, and C, is higher by 0.6 ± 0.4 eV than the electron spectroscopy for chemical analysis (ESCA) value²⁶ of the 3p_{3/2} ionization potential. This discrepancy reflects again the approximate character of Eq. (1), though the calibration uncertainty may also contribute to it. As for E'_0 , it is larger than the ESCA value by 0.3 ± 0.2 eV.

C. Solid Kr

The peak positions and thresholds observed in the spectra of solid Kr are summarized in Table II. The similarity with the spectrum in the gas phase implies assigning the lines to two spin-orbit split series, one including peaks A and B and the other A' and B'. The two parts were analyzed by means of the effective-mass model, usually employed for Mott-Wannier valence exciton series in solids:

$$E_n = E_0 - \frac{b}{n^2}, \quad n = 1, 2, \dots, \quad (2)$$

$$b = \frac{\mu_{\text{exc}} R}{\epsilon^2}. \quad (3)$$

Here μ_{exc} is the reduced effective mass of the exciton (in terms of the free-electron mass) and ϵ the dielectric constant. The effective Rydberg constant b was assumed to be equal in both series;¹⁷ for the second series, E_0 above is replaced by E'_0 . The agreement found between calculated and experimental peak positions (Table II) does not imply high reliability of the model, since only two peaks were observed in each series. Note also that in the Mott-Wannier *valence* exciton series in rare-gas solids the $n = 1$ line does not fit well Eq. (2) and central-cell corrections have to be applied.^{17,32} Because of the insufficiency of the data, this point could not be checked, of course, in the present case. We point out that the value $b = 2.8 \pm 0.2$ eV is considerably higher than the value $b = 1.4$ eV obtained for the valence excitons.^{17,32} This will be discussed further on.

The spectra were analyzed on the basis of the Rydberg model of Eq. (1) as well, following a suggestion by Resca and Resta,³³ who showed that a good empirical fit to *all* lines of the valence exciton series in rare-gas solids can be obtained by adjusting the values of all three constants, E_0 , R , and Δ in Eq. (1). We calculated E_0 , Δ , E'_0 (the latter referring to the second series), keeping for R its gas-phase value. The parameters turned out to be close to those in the gas phase (Table II). The agreement with the observed peak positions is very good, but, because of the small number of peaks observed, this is again no indication for the reliability of the model. The coincidence of the respective peak positions as calculated by the two models is fortuitous. In Sec. III F of this paper both models are critically discussed.

Line *a* (Fig. 1; Table II) at 207.8 eV is probably an artifact, since it is very weak. Alternatively, it might perhaps be a manifestation of many-body effects known from ESCA spectra.²⁶ If so, the small deviation from the fitted main peak in the same region of the gas-phase spectrum (Fig. 1) should be regarded as a real one and interpreted similarly.

It can be seen in the solid Kr spectra of Fig. 1 that at the energy marked *L* the decay of the intensity becomes (rather abruptly) slower and that at *L'* there is even a slight intensity rise. *L* and *L'* are identified as photoconduction threshold energies. Table II shows that the values of *L* and *L'* are very near to those of the series limits E_0 and E'_0 respectively, as calculated by the model of Eq. (1). Now the value of a series limit like E_0 or E'_0 in a solid indicates the minimum energy needed to release an electron into the conduction band; the correspondence of E_0 and E'_0 with *L* and *L'*, respectively, is a very clear confirmation of this interpretation. Correspondence between series limit and photoconduction threshold is well known in the valence regime, for Mott-Wannier exciton series,¹⁵ but the present report to our knowledge seems to be the first one to show such a correspondence for *core exciton series* of any solid.

It should be noted that the thresholds *L* and *L'* appear not only in the photoconduction excitation spectrum, but in the photoemission yield spectrum as well, even though the vacuum level in solid Kr is above the bottom of the conduction band by about 0.3 eV (Ref. 32) and thus electrons at the bottom of the band cannot escape. Moreover, Fig. 1 shows that for solid Kr the photoemission yield spectrum is almost identical with the photoconduction spectrum, though the former is due to electrons that leave the sample and the latter

is a record of those that are collected by the positive sample electrode. For the resonant excitations, i.e., the peaks A, B, A', B' , this is not surprising, since for them the majority of electrons contributing to the signals comprises those that are liberated in the course of the Auger and Coster-Kronig decay of the core hole as well as their various secondaries. This has been demonstrated for the gas^{11,12,31} and can be safely assumed to be true for the solid as well. Since each member of a series is associated with the same core level, the contribution of the electrons originating in the core hole decay to photoemission and to photoconduction, respectively, is independent on the particular resonant state that had been excited. Even so, as pointed out above, differences between the two kinds of spectra could be expected to appear at direct ionization thresholds: the direct contribution to photoconduction should occur at a somewhat lower energy than that to the photoemission. However, the direct photoconduction thresholds L and L' could be clearly observed only because the density of states in the conduction band has a maximum at the bottom of the band.³² This high density of states implies increases of the absorption cross section at L and L' . Thus at these energies the creation of core holes is also enhanced and therefore more electrons of the core decay processes are released. Contribution from these electrons becomes manifest at L and L' in the photoemission yield spectrum. On the other hand, the onset of *direct* transitions from the sample into the surrounding *vacuum* does not show in either the gas spectrum or in the photoemission yield spectrum of the solid, probably since the number of the directly released electrons is very small in comparison with the number of electrons from other sources. The overall situation is simpler in the case of solid xenon (see below).

As for the linewidths, it can be seen from Table II that $w_0(A) = w_0(A') = 1.5 \pm 0.2$ eV; $w_0(B) = 2.1 \pm 0.2$ eV and $w_0(B') = 2.7 \pm 0.2$ eV. B and B' in the solid are appreciably broader than in the gas. Moreover, in the solid—but not in the gas— B' is both broader and higher than A' . One would definitely expect final-state broadening in the solid, mainly because of the effect of phonons.²³ For example, for Kr at the $3d$ edge this amounts to 30 meV;¹⁰ for the first bulk valence line in Kr ($4p^5 5s$ in the gas phase) it is 80 meV.³⁴ In the present case, the effect of the solid-state environment seems to be stronger and differs considerably from line to line. We strongly suspect that partial, unresolved overlapping with transitions to $4d$ and $4d'$ and perhaps even with higher members of the ns and ns' series are at play. The effect of the solid state has been considered on the $3s$ and $3p$ linewidths from Kr to Xe (Ref. 35, and reference therein), but no theoretical calculation of the linewidths of the resonant excitations discussed in this paper seem to exist for solid rare gases.

D. Xe gas

An inherent difficulty was encountered in this case when trying to separate the contributions of the $4p$ excitations, i.e., when looking for a “correct” baseline. The baseline marked $B12$ in the inset for Xe gas (Fig. 2) coincides with the spectrum of Fig. 2 below ~ 140.2 eV and it is an exponential extrapolation of it beyond this photon energy. Using scaled values of the atomic absorption cross section,³⁶ along with a

small linear bolometric correction, results in a very close approximation of this curve. However, this baseline ignores the clear increase of the average trend of the spectrum above ~ 142.5 eV. In this region a horizontal baseline seems to be the correct one— $B11$ is drawn in accord with this observation. It is highly probable that the change of the average trend has to be attributed to many-body effects. ESCA studies in the region above ~ 145 eV and extending for several tens of eV revealed a considerable increase of the continuous background, with numerous peaks of various sizes superimposed.²⁶ These features were explained by invoking many-body effects^{37,38} that arise mainly since in this region double ionization of the $4d$ shell becomes possible; theory closely agrees with the shape of the continuum.^{37,38} While the features just mentioned involve *ionization*, it is likely that in our case double *excitation* of $4d$ is at play, along with contribution with the low-energy tail of the totally smeared out $4p_{1/2}$ edge (see below). The main graph and the data of Table III for Xe gas are based on the subtraction of $B11$, but, for comparison, the graph obtained by subtracting $B12$ (not shown) was also constructed and analyzed.

The Xe spectra for both phases (Fig. 2) exhibit only one series of lines, with monotonically decreasing intensities, in contrast with the case of krypton. Some of these lines in the gas phase were reported by previous authors and assigned^{2,25,39,40} to transitions from the $4p_{3/2}$ subshell. No structure attributed to transitions from the $4p_{1/2}$ subshell has been reported to our knowledge. We note that according to Δ SCF (relativistic, modified Hartree-Fock-Slater method)⁴¹ theoretical estimates the $4p_{1/2}$ ionization potential should be 12.5 eV above the $4p_{3/2}$ threshold, but ESCA experiments did not reveal any trace of it;²⁶ this fact was fully accounted for by super-Coster-Kronig decay, shortening drastically the lifetime.^{26,38,42} Indeed, in the course of the present experiments no structure was found beyond 146 eV up to 160 eV (not shown).

Table III shows the peak positions of the $4p_{3/2}$ series in Xe gas. Previous experimental results by other authors^{25,39,40} are also shown; the differences seem to be mainly due to calibration errors in previous works, especially in the earliest ones. The positions of the main lines A – D are compared with theory based on the Tamm-Dancoff approximation;^{14,42} the agreement between theory and experiment is reasonable, though some of the deviations are significant, not attributable to experimental error.

The assignment of the lines in Table III is in accord with Ohno's theoretical calculation^{14,42} and Refs. 39 and 40 and at variance with Ref. 25. We also point out that according to the present assignment the energy intervals between adjacent Xe $4p^5 ns$ core Rydberg states are approximately equal to the energy intervals of the Cs $5p^6 ns$ states and those of the Xe $5p^5 ns$ states. For example, the total range (from A to the series limit) of the $4p^5 ns$ series is 4.15 eV; the corresponding range of the Cs $5p^6 ns$ spectrum is 3.89 eV (Ref. 27) and of the Xe $5p^5 ns$ spectrum 3.7 eV.²⁷ In Ref. 25 no line is assigned to the $6s$ transition.

Table III also shows peak positions calculated according to the Rydberg model with constant quantum defect, Eq. (1), $n = 6$ – 10 . It can be seen that the model fits reasonably well the experimental results (lines A – E), though again, some of

TABLE III. Energies, linewidths, and assignments in the TTY spectrum of 4*p* excited Xe gas. Calibration uncertainty, ± 0.2 eV, relative position uncertainty, ± 0.05 eV.

Feature	Energy, experimental		Energy, calculated Eq. (1)			Assignment	FWHM	
	This work	Other works	Energy, theory	This work ^a	Other works		Expt.	Theory ^b
A	141.55	142.5 ^c	141.75 ^e	141.48		4 <i>p</i> ⁵ 6 <i>s</i>	0.52 \pm 0.02 ^f	0.9
		142.0 ^d						
B	143.77	144.47 ^c	143.93 ^e	143.95		4 <i>p</i> ⁵ 7 <i>s</i>	0.59 \pm 0.03 ^f	
		144.1 ^d						
C	144.54	144.6 ^g	144.65 ^e	144.76		4 <i>p</i> ⁵ 8 <i>s</i>	0.54 \pm 0.03 ^f	
D	145.18		144.96 ^e	145.13		4 <i>p</i> ⁵ 9 <i>s</i>	0.51 \pm 0.03 ^f	
E	145.66			145.32		4 <i>p</i> ⁵ 10 <i>s</i>	0.40 \pm 0.04 ^f	
a	141.10						0.74 \pm 0.05 ^f	
b	142.07						0.64 \pm 0.03 ^f	
c	143.20		142.89 ^e			4 <i>p</i> ⁵ 5 <i>d</i> _{3/2} or 4 <i>p</i> ⁵ 5 <i>d</i> _{1/2}	0.59 \pm 0.05 ^f	
<i>E</i> ₀		145.51 ^h	144.2 ^b	145.7 \pm 0.2	145.6 \pm 0.5 ^d 145.5 \pm 0.2 ^e	4 <i>p</i> _{3/2} threshold	0.33 \pm 0.03 ⁱ	0.6

^a $\Delta = 4.21 \pm 0.06$.

^bReference 42.

^cReference 39.

^dReference 40.

^eReference 14, taking $E_0 = 145.51$ eV (Ref. 26).

^fThis work.

^gReference 25.

^hReference 26.

ⁱReference 43.

the deviations are not negligible. The series limit E_0 obtained from the fit is equal, within the calibration uncertainty, to the ESCA value.^{26,43}

The spectrum was decomposed into Gaussians. The unexpected and hitherto unreported peaks *a* and *b* are manifest as shoulders on the two flanks of the main peak *A*. Their presence and positions have been consistently confirmed in repeated experiments. Very tentatively, we consider *a* and *b* to be analogous to small peaks in the ESCA spectra; near the main peak at 145.63 eV.⁴³ The many-electron effects underlying this structure have been investigated in depth (e.g., Refs. 38, 44, and 45); the first detailed assignment of these lines was made recently by Kivimäki *et al.*,⁴³ based on their combined experimental study by means of ESCA and Auger spectroscopy. As for peak *c*, it might be due to transition to 5*d*_{3/2} or to 5*d*_{1/2}, but one cannot rule out the possibility that it is just a correction necessary because of the assumed Gaussian shape of peak *B*. Table III includes the linewidths determined in this work as well as comparison with recent theoretical results by Ohno.⁴² The instrumental contribution to these widths is negligible.

Comparing to the above data the results of the fitting with baseline *B12* subtracted, we found that there is no change in the positions of peaks *A*, *B*, and *C*. *D* is upshifted by 0.04 and *E* by 0.08 eV. The series limit becomes $E_0 = 145.8 \pm 0.2$ eV, the quantum defect is $\Delta = 4.22 \pm 0.08$. Comparing with the data of Table III, one sees that even a drastic change of the baseline has only a very slight effect on the main

conclusions. As for the widths, that of *A* remains unchanged, but the other main peaks broaden appreciably, namely by 0.04 to 0.15 eV.

E. Solid Xe

The only published absorption spectrum of solid Xe in the 4*p* threshold region is by Haensel *et al.*² In Fig. 3 of Ref. 2 two small peaks can be seen between 142–144 eV. They were assigned to core excitons below the 4*p*_{3/2} threshold. The presence and assignment of these peaks is confirmed in this work. Two more, broader lines were reported in Ref. 2 between 148.5–153.5 eV, assigned tentatively to core excitons below the 4*p*_{1/2} edge; our solid-Xe spectra did not cover this energy region.

Several differences were observed between the photoemission yield and the photoconduction excitation spectra for solid Xe (Fig. 2). First, the peaks *C* and *D* are clearly observable in the photoemission spectrum, but they are washed out in the photoconduction spectrum. Imperfect crystallinity, affecting more the photoconduction spectrum, might be the cause for this difference. Second, the peak *a* at 143.0 eV stands out more clearly in the photoconduction spectrum than in the photoemission spectrum. This peak is probably associated with transition to the 5*d*_{3/2} or 5*d*_{1/2} state. However, the most interesting difference is the fact that in the photoconduction spectrum there is a clear rise at 145.1 eV (marked by *L*), while in the photoemission spectrum there is only a moderate rise of the slope at this energy.

TABLE IV. Experimental and calculated features in the photoemission yield and photoconduction excitation spectra of $4p$ excited solid Xe and comparisons with valence exciton energies. Calibration uncertainty, ± 0.2 eV; relative position uncertainty, ± 0.05 eV.

Feature	Energy, experimental		Energy, calculated			Energy, valence exciton ^a	FWHM
	This work	Ref. 2	By Eq. (2) ^b	By Eq. (2) ^c	By Eq. (1) ^d		
<i>A</i>	142.11	142.1	142.24		142.07	8.37	0.85 ± 0.01
<i>B</i>	143.69	143.8	144.25	143.62	143.78	9.07	0.85 ± 0.01
<i>C</i>	144.31		144.61	144.47	144.41	9.21	0.44 ± 0.02
<i>D</i>	144.90		144.74	144.77	144.71		0.44 ± 0.02
<i>a</i>	143.00						1.0 ± 0.02
<i>L</i>	145.1						
E_0			144.9 ± 0.3	145.2 ± 0.3	145.2 ± 0.1	9.33	

^aReference 32.

^bEquation (2), by fitting to *A*, *B*, *C*, and *D*; $b = 2.7 \pm 0.7$ eV.

^cEquation (2), by fitting to *B*, *C*, and *D* (see text); $b = 6.0 \pm 1.6$ eV.

^dEquation (1), with $\Delta = 3.9 \pm 0.1$.

The series of peaks *A–D* was analyzed by means of the most often employed model for valence Mott-Wannier excitons, namely, the effective-mass model of Eq. (2). Table IV shows that the model represents approximately the peak positions for these core exciton peaks as well; the deviations are, however, certainly significant. Accordingly, the series limit E_0 and the effective Rydberg constant b were determined with appreciable uncertainties: $E_0 = 144.9 \pm 0.3$ eV and $b = 2.7 \pm 0.7$ eV. The value of L falls within the limits of the estimate for E_0 . Again, as in the case of solid Kr presented above, the correspondence between E_0 , determined from spectroscopic data, and the abrupt rise in photoconduction, is simple and direct evidence for the validity of the phenomenological interpretation of the spectral series. The Xe case is even more clear cut, since E_0 is determined from the position of four lines instead of two in the Kr case, and the rise is much more prominent in the photoconduction spectrum than in the photoemission yield spectrum.

Even so, the value of b is much too high if the known values of the parameters in Eq. (3) are used: we have $1/\mu_{\text{exc}} = 1/\mu_e + 1/\mu_h$, where μ_e is the effective electron mass at the bottom of the conduction band and μ_h is the effective mass of the coupled hole (both in units of the free electron mass). In a precise recent work on image states and quantum wells in thin-Xe layers it was found that $\mu_e = 0.57$.⁴⁶ Since the core hole is immobile, in the present case $\mu_{\text{exc}} = 0.57$. Accordingly, substituting for ε the optical dielectric constant⁴⁷ $\varepsilon = 2.24$, Eq. (3) would result in $b = 1.54$ eV. Such a large discrepancy between b as obtained from analyzing the experiment and that calculated by means of Eq. (3) was pointed out above for the case of Kr as well and clearly indicates the inadequacy of the effective mass approximation for the core excitons observed. Further discussion of this point will follow below.

The applicability of Eq. (2) to the results on solid xenon was checked in one more manner, namely, by fitting it to the *three* peaks *B*, *C*, and *D* only with Eq. (2) ($n = 2, 3, 4$), as customary for valence excitons in rare-gas solids^{17,32} (for the $n = 1$ exciton central cell corrections are applied in the valence case). However, this procedure furnished an unlikely high value for b (Table IV).

As in the case of solid Kr, the data have been fitted to the Rydberg model [Eq. (1), with constant quantum defect] as well. Table IV clearly shows that this is a considerably better fit than that of Eq. (2). It should be stressed that the values for E_0 obtained by the different models are all in accord with identifying the onset *L* of direct photoconduction with the series limit.

The threshold energy I for direct photoionization can be found from the relationship $I = L - V_0$, V_0 denoting the energy of the bottom of the conduction band with respect to the vacuum level. From absorption and photoconductivity measurements in the valence region it is known that $V_0 \approx -0.4$ eV,³² leading to $I = 145.5$ eV. As in the case of Kr, there is no indication in the photoemission yield spectrum to the onset of direct transitions into the surrounding vacuum.

The peak positions reported above are based on the decomposition of the photoemission yield spectrum into Lorentzians: decomposition into Gaussians resulted in a definitely poorer fit. The full widths at half height found are also listed in the table; no comparable theoretical results seem to exist.

F. Core excitons

The following discussion applies to both solids, Kr and Xe, though for Xe the evidence is clearer and more detailed.

Theories of core excitons^{48–50} do not usually deal with *series* of lines like the ones recorded in this study. We recall that the peak positions in the present data can be approximated either by means of the simple Rydberg model [Eq. (1)], with parameter values not far from those in the gas phase, or else by means of the Mott-Wannier exciton model [Eq. (2)], with binding energies considerably higher than those of the respective valence Mott-Wannier excitons; the fit of the latter model is worse. However, neither one of the two empirical models is really satisfactory. For the first [Eq. (1)], the gas-phase Rydberg constant is employed, although in the solid phase the higher orbitals encompass many other atoms. For the second model, the value of the binding energy is considerably larger than expected from the value of the known effective electron mass and dielectric constant ε . We

mention in passing that a combination of the two models, as suggested by Resca and Resta³³ brings no improvement. On the contrary, if one substitutes $n + \delta$ with $\delta > 0$ for n in Eq. (2), the effective Rydberg constant b becomes even larger and the fit is worse.

It should be emphasized that the difficulty is indeed basic, independent of any model: the essential fact is that the term values (or binding energies) of the core excitations observed in the rare-gas solids are very near to those in the respective gases, but considerably larger than the term values of the corresponding excitations from the valence band. Hjalmarson, Büttner, and Dow⁴⁹ and Bassani⁵¹ discussed in detail a closely related problem, namely, the fact that binding energies of core excitons in many *semiconductors* are much larger than the binding energies of the corresponding valence excitons. Bassani⁵¹ presented detailed theoretical calculations investigating the possible reasons for this effect, involving the breakdown of the effective-mass approximation [our Eqs. (2) and (3)]. Calculations on dynamical correlation effects by means of electron polaron theory showed that such a breakdown—and thus an explanation for the binding energy discrepancy—cannot occur in semiconductors, because of their high dielectric constants and low effective electron masses. It does occur, however, for the $n = 1$ exciton (but not for the higher ones) in solid Ar. Other rare-gas solids are not mentioned in Ref. 51 but since solid Kr and Xe have higher dielectric constants and lower effective masses than solid Ar, dynamical correlation effects should be unimportant for $n \geq 2$ in these solids. Bassani leaves the problem open and emphasizes that experimental observation of core exciton *series* and determination of ionization thresholds could lead to firmer conclusions. The present work fulfills these requirements and furnishes gas-phase data as well for comparison.

Resca, Resta, and Rodriguez formulated a nonstructural theory for excitons in rare-gas solids, closely associating gas-phase Rydberg and solid-phase exciton features.⁵² Applying the theory to the two $4p_{3/2}$ core exciton lines in solid Xe reported by Haensel *et al.*,² they obtained $\mu_{\text{exc}} = 0.65$ and $E_0 = 143.88$ eV.⁵³ The results of the present work could serve as a much more stringent test for the model, since (i) more lines are now known, with higher accuracy, both for the gas and the solid; (ii) there is direct independent evidence about the value of the photoconductivity threshold, and (iii) the effective electron mass is known.⁴⁶ It follows that, in principle, the nonstructural theory could be tested on the basis of the results reported here without any adjustable parameters. Criticism of the model has concerned its central assumption, treating excitons as solid-state variants of Rydberg

states in the gas.⁵⁴ It was based on experimental facts pertaining to rare-gas fluids. Evidence showed that *valence* excitons evolve quite differently with fluid density than atomic lines: higher Rydberg states wash out and disappear with increasing density, while the excitonic lines start to appear only at densities of the same order of magnitude as that of the solid. Even the $n = 1$ exciton, which is largely Frenkel-type, is quite distinct from the neighboring, strongly broadened, and somewhat shifted atomic $6s$ line.^{55–57} However, this clear distinction between Rydberg states in the gas and Mott-Wannier excitons in the dense fluid and the solid has been demonstrated only for *valence* excitations.^{55–57} The *core* excitons discussed in this work lack the most characteristic property of excitons, namely mobility, because of the vanishing overlap of core hole functions on neighboring atoms. To a large extent, this fact might cancel the arguments of Ref. 54 for core excitons. It is conceivable that series of experiments on clusters of increasing size, or on fluids with increasing density, might show the core excitons evolving gradually and continuously from the Rydberg states, in contrast with the valence case. Xenon seems to be again a preferred substance for such studies, mainly because only one of the split-orbit series appears, though the many-body effects observed in the gas-phase spectra may cause difficulties of interpretation.

IV. CONCLUSIONS

The core exciton series of lines observed in solid Kr below the $3p_{3/2}$ and $3p_{1/2}$ thresholds and in solid Xe below the $4p_{3/2}$ threshold are described by means of parameters with values near to those of Rydberg series in the respective gases. In contrast, the parameters of the core exciton series are unrelated to the parameters of the Mott-Wannier valence excitons in the same solid. While the results presented indicate that atomic structure has a more dominant effect on the excitations reported than the crystalline environment, the values of the parameters cannot be simply interpreted, and deeper theoretical treatment is required.

ACKNOWLEDGMENTS

Financial support by the Deutsche Forschungsgemeinschaft (DFG) and the Fonds der Chemischen Industrie is gratefully acknowledged. The authors acknowledge with thanks most useful discussions with M. Ya. Amusia, B. Laikhtman, and N. Zeldes in Jerusalem and with P. A. Dowben in Lincoln, NE.

*Present address: LURE, F-9989, Orsay, France.

¹R. Haensel, G. Keitel, P. Schreiber, and C. Kunz, Phys. Rev. Lett. **22**, 398 (1969).

²R. Haensel, G. Keitel, P. Schreiber, and C. Kunz, Phys. Rev. **188**, 1375 (1969).

³R. Haensel, G. Keitel, N. Kosuch, U. Nielsen, and P. Schreiber, J. Phys. (Paris) Colloq. **32**, C4-236 (1971).

⁴R. Haensel, N. Kosuch, U. Nielsen, U. Rössler, and B. Sonntag, Phys. Rev. B **7**, 1577 (1973).

⁵E. Rühl, H. W. Jochims, C. Schmale, E. Biller, A. P. Hitchcock,

and H. Baumgärtel, Chem. Phys. Lett. **178**, 558 (1991); E. Rühl, C. Heinzl, A. P. Hitchcock, and H. Baumgärtel, J. Chem. Phys. **98**, 2653 (1993).

⁶E. Rühl, C. Heinzl, and H. W. Jochims, Chem. Phys. Lett. **211**, 403 (1993).

⁷O. Björneholm, F. Federmann, F. Fössing, and T. Möller, Phys. Rev. Lett. **74**, 3017 (1995).

⁸O. Björneholm, F. Federmann, F. Fössing, and T. Möller, J. Chem. Phys. **104**, 1846 (1996).

⁹E. Rühl, A. P. Hitchcock, P. Morin, and M. Lavollée, J. Chim.

- Phys. Phys.-Chim. Biol. **92**, 521 (1995).
- ¹⁰A. Knop, B. Wassermann, and E. Rühl, Phys. Rev. Lett. **80**, 2302 (1998).
- ¹¹D. Menzel, Appl. Phys. A: Solids Surf. **A51**, 163 (1990).
- ¹²W. Wurth, G. Rocker, P. Feulner, R. Scheuerer, L. Zhu, and D. Menzel, Phys. Rev. B **47**, 6697 (1993).
- ¹³G. C. King, M. Tronc, F. H. Read, and R. Bradford, J. Phys. B **10**, 2479 (1977).
- ¹⁴M. Ohno, Phys. Rev. A **51**, 1042 (1995).
- ¹⁵U. Asaf and I. T. Steinberger, Phys. Rev. B **10**, 4464 (1974); R. Reininger, U. Asaf, I. T. Steinberger, P. Laporte, and V. Saile, *ibid.* **26**, 6294 (1982).
- ¹⁶R. Reininger, S. Bernstorff, P. Laporte, and I. T. Steinberger, Chem. Phys. **86**, 189 (1984); R. Reininger, V. Saile, P. Laporte, and I. T. Steinberger, *ibid.* **89**, 473 (1984).
- ¹⁷See, e.g., B. Sonntag, in *Rare Gas Solids*, edited by M. K. Klein and J. A. Venables (Academic, London, 1977), Vol II, p. 1021.
- ¹⁸S. Bernstorff, W. Braun, M. Mast, W. Peatman, and T. Schroeder, Rev. Sci. Instrum. **60**, 2097 (1989).
- ¹⁹W. B. Peatman, J. Bahrtdt, F. Eggenstein, G. Reinhardt, and F. Senf, Rev. Sci. Instrum. **66**, 2801 (1995).
- ²⁰K. H. Sze and C. E. Brion, Chem. Phys. **140**, 439 (1990); J. T. Francis, C. C. Turci, T. Tyliczszak, G. G. B. de Souza, N. Kosugi, and A. P. Hitchcock, Phys. Rev. A **52**, 4665 (1995).
- ²¹E. Rühl, C. Heinzl, H. C. Schmelz, and C. Reynaud (unpublished).
- ²²D. Blechschmidt, R. Haensel, E. E. Koch, U. Nielsen, and T. Sagawa, Chem. Phys. Lett. **14**, 33 (1972).
- ²³G. Zimmerer, in *Excited State Spectroscopy in Solids*, edited by U. M. Grassano and N. Terzi (North-Holland, Amsterdam, 1987), p. 37.
- ²⁴W. S. Watson and F. J. Morgan, J. Phys. B **2**, 277 (1969).
- ²⁵T. Hayaishi, Y. Marioka, T. Akahori, M. Watanabe, A. Yagishita, and M. Nakamura, Z. Phys. D **4**, 25 (1986).
- ²⁶S. Svensson, N. Mårtensson, E. Basilier, P. Å. Malmquist, U. Gelius, and K. Siegbahn, Phys. Scr. **14**, 141 (1976); S. Svensson, B. Eriksson, N. Mårtensson, G. Wendin, and U. Gelius, J. Electron Spectrosc. Relat. Phenom. **47**, 327 (1988).
- ²⁷C. E. Moore, *Atomic Energy Levels*, Natl. Bur. Stand. (U.S.) Circ. No. 467 (U.S. GPO, Washington, D.C., 1952); Vol. II; Vol. III (1958).
- ²⁸M. Ohno and G. Wendin, J. Phys. B **11**, 1557 (1978).
- ²⁹P. L. Lee, Nucl. Instrum. Methods **144**, 363 (1977).
- ³⁰M. Ohno and G. Wendin, Phys. Rev. A **31**, 2318 (1985); M. Ya. Amusia, *Atomic Photoeffect* (Plenum, New York, 1990).
- ³¹J. Jauhiainen, A. Kivimäki, S. Aksela, O-P. Sairanen, and H. Aksela, J. Phys. B **28**, 4091 (1995).
- ³²N. Schwentner, E. E. Koch, and J. Jortner, *Electronic Excitations in Condensed Rare Gases* (Springer, Berlin, 1985).
- ³³L. Resca and R. Resta, Phys. Rev. B **19**, 1683 (1979).
- ³⁴V. Saile, Appl. Opt. **19**, 4115 (1980).
- ³⁵M. Ohno, Phys. Rev. B **29**, 3127 (1984).
- ³⁶B. L. Henke, E. M. Gullikson, and J. C. Davis, At. Data Nucl. Data Tables **54**, 181 (1993).
- ³⁷M. Ya. Amusia, N. A. Cherepkov, and L. V. Chernysheva, Zh. Eksp. Teor. Fiz. **60**, 160 (1971) [Sov. Phys. JETP **33**, 90 (1971)].
- ³⁸G. Wendin and M. Ohno, Phys. Scr. **14**, 148 (1976).
- ³⁹A. P. Lukirskii, T. M. Zimkina, and I. A. Brytov, Bull. Acad. Sci. USSR, Phys. Ser. **28**, 681 (1965).
- ⁴⁰K. Codling and R. P. Madden, Appl. Opt. **4**, 1431 (1965).
- ⁴¹A. Rosén and I. Lindgren, Phys. Rev. **176**, 114 (1968).
- ⁴²M. Ohno, J. Electron Spectrosc. Relat. Phenom. **71**, 25 (1995).
- ⁴³A. Kivimäki, H. Aksela, J. Jauhiainen, M. Kivilompolo, E. Nõn-miste, and S. Aksela, J. Electron Spectrosc. Relat. Phenom. **93**, 89 (1998).
- ⁴⁴M. Ohno, Phys. Scr. **21**, 589 (1980).
- ⁴⁵M. Ohno and G. Wendin, Z. Phys. D **5**, 233 (1987).
- ⁴⁶J. D. McNeill, R. L. Lingle, Jr., R. E. Jordan, D. F. Padowitz, and C. B. Harris, J. Chem. Phys. **105**, 3883 (1996).
- ⁴⁷A. C. Sinnock and B. L. Smith, Phys. Rev. **181**, 1297 (1969).
- ⁴⁸M. Altarelli, W. Andreoni, and W. Bassani, Solid State Commun. **16**, 143 (1975).
- ⁴⁹H. P. Hjalmarsen, H. Büttner, and J. D. Dow, Phys. Rev. B **24**, 1683 (1979).
- ⁵⁰A. Zunger, Phys. Rev. Lett. **50**, 1215 (1983).
- ⁵¹F. Bassani, Appl. Opt. **19**, 4093 (1980).
- ⁵²L. Resca, R. Resta, and S. Rodriguez, Phys. Rev. B **18**, 696 (1978).
- ⁵³L. Resca, R. Resta, and S. Rodriguez, Phys. Rev. B **18**, 702 (1978).
- ⁵⁴V. Saile, R. Reininger, P. Laporte, I. T. Steinberger, and G. L. Findley, Phys. Rev. B **37**, 10 901 (1988).
- ⁵⁵P. Laporte and I. T. Steinberger, Phys. Rev. B **15**, 2538 (1977).
- ⁵⁶P. Laporte, J. L. Subtil, U. Asaf, I. T. Steinberger, and S. Wind, Phys. Rev. Lett. **45**, 2138 (1980).
- ⁵⁷P. Laporte, J. L. Subtil, R. Reininger, V. Saile, S. Bernstorff, and I. T. Steinberger, Phys. Rev. B **35**, 6270 (1987).